# Extensive differential protein phosphorylation as intraerythrocytic *Plasmodium falciparum* schizonts develop into extracellular invasive merozoites

Edwin Lasonder[1,*], Judith L. Green[2], Munira Grainger[2], Gordon Langsley[3,4,*], Anthony A. Holder[2,*]

[1]School of Biomedical and Healthcare Sciences, A405 Portland Square, Plymouth University, Drake Circus, Plymouth, Devon PL4 8AA, United Kingdom.

[2]Division of Parasitology, MRC National Institute for Medical Research, The Ridgeway, Mill Hill, London, NW7 1AA, United Kingdom.

[3]Laboratoire de Biologie Cellulaire Comparative des Apicomplexes, Faculté de Médicine, Université Paris Descartes - Sorbonne Paris Cité, France.

[4]Inserm U1016, CNRS UMR8104, Institut Cochin, Paris, 75014 France.

*Corresponding authors

**Abstract**

Pathology of the most lethal form of malaria is caused by *Plasmodium falciparum* asexual blood stages and initiated by merozoite invasion of erythrocytes. We present a phosphoproteome analysis of extracellular merozoites revealing 1765 unique phosphorylation sites including 785 sites not previously detected in schizonts. The observed differential phosphorylation between extra and intraerythrocytic life cycle stages was confirmed using both phospho-site and phospho-motif specific antibodies and is consistent with the core motif [K/R]xx[pS/pT] being highly represented in merozoite phosphoproteins. Comparative bioinformatic analyses highlighted protein sets and pathways with established roles in invasion. Within the merozoite phosphoprotein interaction network a sub-network of 119 proteins with potential roles in cellular movement and invasion was identified and suggested that it is co-regulated by a further small sub-network of protein kinase A (PKA), two calcium-dependent protein kinases (CDPKs), a phosphatidyl inositol kinase (PI3K) and a GCN2-like eIF2-kinase with a predicted role in translational arrest and associated changes in the ubquitinome. To test this notion experimentally, we examined the overall ubiquitination level in intracellular schizonts versus extracellular merozoites and found it highly upregulated in merozoites. We propose that alterations in the phosphoproteome and ubiquitinome reflect a starvation-induced translational arrest as intracellular schizonts transform into extracellular merozoites.

## 1. Introduction

The most lethal form of human malaria is caused by *Plasmodium falciparum*. This parasite has a complex life cycle in both mosquito and human host, where asexual multiplication and development within red blood cells (RBC) is responsible for disease pathology. Intra-RBC parasite development is initiated by merozoite invasion of erythrocytes, as merozoites are first released into the blood stream from merosomes in the liver [1] and subsequently released at the end of each cycle of multiplication in RBC. Preventing blood stage infection by targeting merozoites is an attractive intervention strategy to develop treatments to alleviate disease. Therefore, understanding merozoite development and the identification of new anti-malarial therapeutic targets are of the utmost importance [2].

The merozoite is well adapted for RBC invasion [3]. It has the pellicular structure typical of members of the Apicomplexa phylum including an apical end with secretory organelles: micronemes, rhoptries and dense granules [4]. RBC invasion is a multi-step process that is initiated by merozoite attachment, followed by reorientation and sequential discharge of the contents of the apical organelles [5, 6]. During erythrocyte entry, a process that is controlled in part by calcium and cAMP fluxes [7, 8], a moving junction is formed between the parasite and host cell surfaces, and parasite proteins are transferred to the newly invaded erythrocyte [8-10]. After invasion the parasite resides within a parasitophorous vacuole and develops from a 'ring' to a trophozoite that degrades host cell haemoglobin and performs DNA synthesis. The onset of mitosis produces the multinucleated schizont, and following cell division individual merozoites

are formed, which are then released at the end of the cycle to infect new RBC [11]. Within erythrocytes the primary amino acid nutrient source for the developing parasite is haemoglobin, which is degraded in the food vacuole. This structure is elaborated anew following invasion [12] and haemoglobin digestion starts only several hours post-invasion [13]. In late stage multinucleated “segmenter” schizonts that have undergone cytokinesis, the food vacuole is 'pinched off' from the developing merozoites. Therefore, merozoites and post-invasion early ring forms are deprived of haemoglobin-derived amino acids for several hours. However, organelle degradation by autophagy likely provides the developing merozoite and early ring stages with some nutrient [14].

Protein kinases, phosphatases and signal transduction pathways are integral to regulation of the parasite life cycle; for example, both merozoite egress from the host cell and erythrocyte invasion are governed by protein phosphorylation [15, 16]. Unravelling protein phosphorylation and signalling pathways in merozoites requires large-scale phosphoproteome studies that are now feasible using mass spectrometry. Significant efforts have been made in recent years to generate phosphoproteome data principally for schizonts, leading to the identification of more than 12,000 unique protein phosphorylation sites [17-22]. Our previous large scale phosphoproteome analysis of *P. falciparum* schizonts by liquid chromatography tandem mass spectrometry (LC-MS/MS) revealed extensive phosphatidylinositol and cAMP-dependent protein kinase (PKA) signalling and identified three novel PKA substrates associated with the glideosome motor complex that is implicated in driving the parasite into the RBC. These data support a role for cAMP as an important regulator of host cell invasion [7, 18].

In this study we present a large-scale analysis of protein phosphorylation in extracellular merozoites and its comparison with established schizont phosphoproteomes to deepen our understanding of merozoite biology. We use bioinformatics to analyse phosphorylation sites and establish a merozoite phosphoprotein interaction network. Reassuringly this revealed a sub-network of merozoite proteins with predicted roles in cellular movement and invasion. Interestingly, it also revealed a smaller sub-network of five kinases known in other cellular systems to regulate starvation-induced translational arrest and autophagy, both of which involve protein ubiquitination [23-26]. We confirm global changes in phosphorylation patterns between schizonts and merozoites using both commercial phospho-site specific antibodies and a specific phosphoprotein antibody. Importantly, we show that differential phosphorylation is linked to highly elevated ubiquitination in merozoites and we propose that alterations in the phosphoproteome and ubiquitinome reflect starvation-induced translational arrest in merozoites.

## 2. Materials and Methods

### 2.1 Parasites.

*P falciparum* 3D7 line parasites were cultured *in vitro* as described previously [27]. Parasite populations were synchronised by treatment with sorbitol, Percoll gradient centrifugation and passage through a magnetic column, allowing the purification of merozoites as described [27, 28].

### 2.2 In solution protease digestion and peptide purification using the Filter Assisted Sample Preparation (FASP) method.

Approximately 2-3 x$10^9$ merozoites were lysed in 1 ml 2 % SDS in 50 mM Tris-HCl pH 7.3 in the presence of phosphatase and protease inhibitors. Halt™ phosphatase inhibitor cocktail (Thermo Fisher) and complete protease inhibitor cocktail (Roche) were used to suppress phosphatase and protease enzymatic activities. The Halt™ phosphatase cocktail is a concentrated solution of sodium fluoride, sodium orthovanadate, sodium pyrophosphate and β-glycerophosphate, and was diluted 100-fold for the final concentration. The complete protease inhibitor cocktail tablet contains AEBSF, aprotinin, bestatin, E-64, leupeptin, pepstatin A and EDTA, and was diluted according to the specifications of the manufacturer. The merozoite lysate was heated to 95ºC for 5 min and further processed according to the FASP protocol [29]. The lysate was divided and transferred to 12 0.5 ml Amicon Ultra 30K spin filter units (30 kDa cut-off, Millipore), each of which was washed with 0.4 ml 8 M urea in 100 mM Tris-HCl pH 8.0 resulting in a final composition of 0.34% SDS and 5.8 M urea, then reduced with 10

mM DTT at room temperature (RT) for 25 min, concentrated by centrifugation at 14,000 *g* and alkylated in the dark with 50 mM iodoacetamide in 100 mM Tris-HCl pH 8.0 containing 8 M urea at RT for 25 min. The samples were concentrated by centrifugation and diluted 10-fold with 100 mM Tris-HCl, 8 M urea, pH 8.0. This step was repeated 6 times to fully remove SDS from the lysate solution. Then, 2.5 µg lysC protease (Wako) per sample was added in 100 mM Tris-HCl, 4 M urea, pH 8.0, and incubated overnight at room temperature. Samples were further diluted with 50 mM ammonium bicarbonate to a final concentration of 2 M urea and then incubated with 5 µg trypsin (Promega) for 18 h. The tryptic digest was acidified in 0.1 % (vol/vol) trifluoroacetic acid (TFA) and the peptides purified and desalted with C18 Hypersil 500 mg SPE columns (Thermo Fisher). Resultant peptides were separated by strong anion exchange (SAX) membrane filters into six fractions on the basis of their isoelectric points. Peptides were eluted stepwise with Britton and Robinson buffer solutions of decreasing pH: 8.0, 6.0, 5.0, and 4.0, respectively, followed by a final elution with 1 % TFA. All peptide fractions were acidified immediately with 0.1 % TFA and then the peptides were purified again using C18 Hypersil 500 mg SPE columns.

**2.3 Phosphopeptide enrichment**.

Peptides obtained from 2-3 x $10^9$ purified merozoites, corresponding to 3 mg protein as determined by a micro BCA protein assay kit (Thermo Fisher) were incubated with Titansphere 10 µm $TiO_2$ beads (GL Sciences, Inc., Japan) to selectively purify phosphorylated peptides, as described for the schizont phosphoproteome analysis [18]. Prior to incubation the $TiO_2$ beads were washed with 80% (vol/vol) acetonitrile, 0.1%

TFA, re-suspended in 30 mg/ml dihydroxybenzoic acid in 80% acetonitrile, 0.1% TFA and diluted 1:4 with 0.1% TFA. Twenty microlitres of the slurry containing about 1 mg beads were added to peptide solutions in 1.5 ml tubes and incubated under continuous shaking for 1-2 h. Afterwards, the bead slurry was transferred to a micro spin column made from a 200 µl precision pipette tip with an inserted 2mm fused silica frit (50 µm internal diameter). Unbound fractions were collected following centrifugation of the spin column and reincubated with freshly prepared $TiO_2$ bead slurry for 1-2 h. This step was performed three times leading to four micro spin columns with $TiO_2$ beads per peptide SAX fraction. The columns were washed three times by centrifugation with 100 µl 30% acetonitrile, 3% TFA, followed by three washes with 100 µl 80% acetonitrile, 0.3% TFA. Bound phosphopeptides were eluted from the beads with 100 µl 5 % $NH_4OH$, 5 % piperidine, and 5 % pyrrolidine [30]. Peptide solutions were then acidified with TFA and the peptides purified with STAGE tips [31] and dissolved in 0.1% TFA and 10 mM EDTA.

**2.4 Liquid chromatography tandem mass spectrometry (LC-MS/MS).**

Tandem mass spectrometry experiments were performed with the linear ion trap cyclotron resonance Fourier transform (LTQ-Ultra FT) mass spectrometer (Thermo Fisher, Bremen, Germany) coupled to the nano EASY LC system (Proxeon, Denmark) with 15 cm 100 µm internal diameter PicoTip columns (New Objective, Woburn, USA) packed with 3 µm Reprosil C18 beads (Dr. Maisch GmbH, Ammerbuch, Germany). Peptides were separated by liquid chromatography using a gradient from 92% buffer A /8% buffer B to 73% buffer A /27% buffer B (where buffer A is 0.5% acetic acid in water

and buffer B is 0.5% acetic acid in acetonitrile) with a flow-rate of 300 nl/min over 90 min. A voltage of 2.2 kV was applied for electrospray ionisation. Data–dependent acquisition was performed for switching automatically between MS, MS2 and phosphoric acid neutral loss triggered MS3 scan modes. Full-scan MS spectra of intact peptides (m/z 350–1500) with an automated gain control accumulation target value of 1,000,0000 ions were acquired in the Fourier transform ion cyclotron resonance cell with a resolution of 50,000. The four most abundant ions were sequentially isolated and fragmented in the linear ion trap by applying collision induced dissociation using an accumulation target value of 10,000, a capillary temperature of 100°C, and a normalized collision energy of 27%. Multi-stage activation was switched on for neutral loss dependent MS3 fragmentation on the masses of phosphoric acid at charge states 2+, 3+ and 4+. The four most abundant ions were sequentially fragmented under identical settings as for MSMS mode with a normalized collision energy of 40 %. A dynamic exclusion of ions previously sequenced within 180 s was applied. All unassigned charge states and singly charged ions were excluded from fragmentation. Sequencing thresholds were set at 500 counts for MS2 and 5 counts for MS3. The mass spectrometry data have been submitted to the ProteomeXchange Consortium (http://proteomecentral.proteomexchange.org).

193 **2.5 Mascot Peptide identification and MaxQuant validation.**

194 Tandem mass spectrometry data were processed using the same procedure we applied
195 previously to the schizont phosphoproteome [18]. Briefly, Mascot generic peak lists
196 were generated by MaxQuant version 1.013.13 (http://maxquant.org//) [32] and
197 submitted to Mascot version 2.2 (Matrix Science) to search the *P. falciparum* database
198 downloaded from http://plasmodb.org/plasmo/ and supplemented with the human
199 International Protein Index (IPI) database (http://www.ebi.ac.uk/IPI) and frequently
200 observed contaminants and concatenated with reversed copies of all entries. The
201 following search parameters were applied: peptide mass 10 ppm, MSMS mass
202 accuracy of 0.5 Da; enzyme cleavage: trypsin allowing 2 miscleavage sites; fixed
203 modification for cysteines by carboxyamidomethylation and variable modifications to
204 enable detection of phosphorylation at serine, threonine and tyrosine; oxidation of
205 methionine; deamidation of glutamine and asparagine and protein N-terminal
206 acetylation. Mascot search results were processed further by MaxQuant [32], where
207 peptides were filtered; requiring a minimal Mascot peptide score of 20 in combination
208 with the probability that the identification is wrong, the posterior error probability (PEP)
209 of 0.025, a minimal charge state of 2 and no more than two variable modifications per
210 peptide. Peptides and proteins with a false discovery rate (FDR) better than l % were
211 accepted. The phosphorylation site localization probability >0.75 was applied to a obtain
212 phosphopeptide FDR of 1 % [33].
213
214

**2.6 Gene ontology analysis**.

All *P. falciparum* gene ontology analyses were performed with the software package Ontologizer [34] (http://compbio.charite.de/index.php/ontologizer2.html), with the following Open Biological Ontology and Gene association components from http://www.geneontology.org: gene ontology v1.2.obo, goslim_generic.obo and Gene_association.GeneDB–Pfalciparum_2011-5-31. The OPI GO terms were taken from and rearranged to a gene association compatible file. Ontologizer was used to identify overrepresented GO terms for the phosphoproteome relative to the background of the *P. falciparum* proteome (~5500 proteins). GO term enrichment was computed by the parent-child union approach and corrected for multiple testing by the Benjamini and Hochberg method, and was considered significant for adjusted p-values lower than 0.05 [34].

**2.7 Motif analysis**.

Phosphorylation sites were categorized by their chemical properties as acidic, basic, proline-directed, tyrosine or other by a decision tree method from [18, 35] as follows: 1/ Get the 6 neighbouring amino acids before and after the phosphorylation site. 2/ pY at position 0 then classify as ‘‘Tyrosine.’’ 3/ P at +1 then classify as ‘‘Proline-directed.’’ 4/ positions +1 to +6 contain more than one D and E residues then classify as ‘‘Acidic.’’ 5/ K or R at position -3 then classify as ‘‘Basic.’’ 6/ D or E at +1, +2, or +3 then classify as ‘‘Acidic.’’ 7/ between -6 and -1 more than 2 K or R residues then classify as ‘‘Basic.’’ 8/ remaining peptides classify as ‘‘Other".

Merozoite phosphorylation motifs were identified using MotifX [36] that tested for motif overrepresentation in phosphorylated peptides with the following parameters: phosphorylation motif window = 13 amino acids, P-value threshold =$1*10^{-4}$ for S and T residues, $1*10^{-3}$ for Y residues, motif fold increase ≥ 2, a motif frequency > 5, and a background of all *P. falciparum* proteins. MotifX analysis was performed for a normal and a degenerate amino acid set. The degenerate amino acid set was enabled for conservative amino acid substitutions within the motif window according to: A=AG, D=DE, F=FY, K=KR, I=ILVM, Q=QN, S=ST, C=C, H=H, P=P, W=W. When different motifs were found for a peptide by the analyses with different amino acid residues, priority was given to the motif with the highest MotifX score. Sequence logos were generated with Weblogo 3 at http://weblogo.threeplusone.com/create.cgi. The motifs were matched to known protein kinase target motifs using CompariMotif [37] at http://bioware.ucd.ie/~compass/biowareweb/Server_pages/comparimotif.php, and matches with the highest scores were considered as potential links between phosphorylation motifs and protein kinases.

**2.8 Phosphorylated protein interaction network analysis**.

The merozoite phosphoproteome interaction network was constructed from all *P. falciparum* protein-protein interaction data with a minimum confidence level of 0.15 downloaded from the STRING database version 9.0 [38] that were matched with the phosphorylated *P. falciparum* proteins identified in this study and visualized in Cytoscape version 2.8.3 [39]. The merozoite phospho-interactome was analyzed for

highly connected nodes with the molecular complex detection (MCODE) clustering algorithm [40] that was available as a Cytoscape plug-in using default parameters.

**2.9 Phospho-site, Phospho-motif and Protein Ubiquitin Western blots**

Antibodies to the peptide PQRKPL*SIEESF based on the sequence of amino acid residues 41 to 52 of myosin tail domain interacting protein (MTIP) and containing a phosphoserine corresponding to Ser47 [41] were prepared in a sheep and purified by affinity chromatography on the phosphopeptide coupled to a solid support (University of Dundee). Late schizonts and merozoites were purified using a magnet and lysed in 30 cell-pellet volumes of NP40 lysis buffer (0.5% Nonidet P40, 150 mM NaCl, 50 mM Tris-HCl pH 8.0) containing protease inhibitors (Roche). Following incubation on ice for 20 min, the soluble protein solution was collected after centrifugation at 15,000 *g* for 20 min at 4ºC. The merozoite lysate was either untreated or treated with Lambda phosphatase (New England Biolabs), using five units phosphatase/µg protein and incubation for 20 min at 30ºC, then the enzyme was heat inactivated at 65ºC for 10 min. Lysates containing approximately 10 µg protein were resolved on 10% NuPAGE Bis-Tris gels in MOPS buffer (Life Technologies) under reducing conditions and the proteins transferred to nitrocellulose using an iBlot system (Life Technologies). The blot was blocked overnight in phosphate buffered saline containing 1% (wt/vol) BSA and 0.2% (vol/vol) Tween-20 (PBST). For western blotting the sheep anti-phosphopeptide antibodies (1 µg/ml) were pre-incubated with 10 µg/ml non-phosphorylated peptide for 1 h at room temperature to deplete antibodies not specific for the phosphoserine and then incubated with the blot. MTIP was also detected with a rabbit anti-MTIP specific antibody that has

been described previously [5]. All antibody dilutions were made in PBST; washes were with the same buffer. After extensive washing, the appropriate horseradish peroxidase (HRP)-conjugated anti-IgG secondary antibodies (Sigma) were used to detect bound antibody using enhanced chemiluminescence (GE Healthcare) and fluorography.

Antibodies recognizing phospho-PKA (motif 3), phospho-PKB/Akt (motif 4), phospho-PKD (motif 11) and phospho-tyrosine motifs were obtained from Cell Signaling Technologies. Schizont and merozoite cell pellets were resuspended in isotonic 0.15% saponin to lyse red blood cell membranes. Parasites were pelleted by centrifugation at 2400 *g* and then schizonts were resuspended in 10 volumes and merozoites in 50 volumes of lysis buffer (0.5% NP40, 150 mM NaCl, 0.5 mM EDTA, 10 mM Tris HCl pH 8.0). Protein concentrations were determined using a detergent-compatible protein assay (DC-protein assay, Biorad), and 10 µg of each sample were resolved on 10% polyacrylamide gels as described above. Following protein transfer to nitrocellulose and blocking overnight, antibodies diluted 1:1000 were added and incubated with the blot for 1 h at room temperature. Bound antibodies were detected with HRP-linked species-specific secondary antibodies (Biorad) at a dilution of 1:5000, as described above.

To analyse ubiquitination in parasites, a time course of late stage schizonts was prepared. Briefly, parasites were synchronized to a 1 h window and harvested at appropriate time points during the cycle. After initial lysis of the RBC membrane using 0.15% saponin followed by centrifugation of the sample at 2400 *g*, parasites were lysed in a buffer containing 4% CHAPS, 1% DTT, 6 M urea, and 2 M thiourea. Samples were subjected to three freeze-thaw cycles, and then centrifuged at 100,000 *g*. The concentration of protein in the supernatant was determined using the Biorad Protein

Assay, and 2 µg samples of each protein fraction were resolved on a 12% NuPAGE Bis-Tris gel in MOPS buffer. Following transfer to nitrocellulose and blocking as described above, an anti mono- and polyubiquitinylated conjugate monoclonal antibody directly conjugated to HRP (FK2H, Enzo Life Sciences) was used at 1000-fold dilution and detected using ECL. CDPK1 was detected using a specific rabbit polyclonal antibody as described previously [41].

## 3. Results

### 3.1 The phosphoproteome of *P. falciparum* merozoites

Free merozoites were purified after release from highly synchronous populations of schizonts [27, 28], and processed for mass spectrometric phosphoproteome analysis by the gel-free protein digestion procedure, Filter Assisted Sample Preparation (FASP). Merozoites were solubilised in 0.34 % SDS/ 5.8M urea and the proteins digested with the proteolytic enzymes lysC and trypsin. Phosphopeptides were affinity-purified using $TiO_2$ beads, and then subjected to liquid chromatography-tandem mass spectrometry (LC-MS/MS) measurements. Peptides were identified by Mascot searches [42] of MS/MS spectra against protein databases comprising all *P. falciparum* and human proteins. Preliminary peptide identifications were validated in reverse database searches using MaxQuant [32], resulting in identification of 1765 *P. falciparum* phosphopeptides with phosphorylation site localization [33] probabilities >0.75 and representing 740 distinct proteins (Figure 1, Table S1). Peptide identification criteria were: a Mascot score greater than 20, posterior error probability (PEP) less than 0.025,

328 and a phosphopeptide False Discovery Rate (FDR) less than 0.01. A small number of
329 phosphorylated human proteins were identified by these validation criteria: 24 proteins,
330 comprising 36 sites (data not shown). Almost all detected merozoite phosphopeptides
331 were mono-phosphorylated (99.6%), which is likely explained in part by the observed
332 bias in enrichment by $TiO_2$ beads for such peptides [43]. The phospho-amino acid
333 distribution of 80% pSer and 19.6% pThr resembled that of our previous analysis of
334 schizonts using similar methodology [18], with 84.4% and 13.2%, respectively. Tyrosine
335 phosphorylation was less frequent in merozoites (0.4 % of phospho-sites) than in
336 schizonts (2.4 %). The observed low frequency of tyrosine phosphorylation in
337 merozoites highlights our stringent validation criteria since *Plasmodium* parasites lack
338 tyrosine kinases. *Plasmodium* proteins are probably phosphorylated by human tyrosine
339 kinases, and we speculate that host tyrosine kinase activity on extracellular merozoites
340 is likely lower than during intracellular schizont development, where we found a
341 frequency of 2.4 %. A comparative analysis of our merozoite data with the combined
342 data representing 12,252 phosphorylation sites derived from schizonts [18-22] revealed
343 a similar distribution in this combined set, with frequencies of 81.8 % (pSer), 14.4 %
344 (pThr), and 3.8% (pTyr), respectively (Figure 1). The merozoite phosphoproteome
345 contained 785 phosphorylated sites (Figure 1) that were not found among the 12,252
346 phosphorylation sites reported for schizonts. Several sites in merozoite proteins
347 implicated in erythrocyte invasion were found to be phosphorylated in both schizonts
348 and merozoites such as S610 of AMA1, and others such as S1240 of Sub2 appear to
349 be specifically phosphorylated in schizonts. However phosphorylation at some sites in
350 such proteins, for example residues 1024, 1246 and 1261 in MSP1; 1299 in EBA181;

and 137, 139, and 296 in RAP1, appears to be specific to the merozoite fraction (Table S1); the functional significance of this is unknown. The proteome data generated in this study comes from a single biological experiment measuring purified merozoites and contains phosphopeptides with not more than 1 % false identifications.

### 3.2 Functional annotation of the merozoite phosphoproteome

The potential relevance of the merozoite phosphoproteome to parasite invasion biology was assessed by functional enrichment analyses of the 740 phosphorylated merozoite proteins relative to the full *P. falciparum* proteome (~ 5500 proteins). Firstly, a comparative GO enrichment analysis was performed on extra (merozoites)- versus intra-erythrocytic (schizonts) life cycle stages to identify any GO terms that were significantly altered for the merozoite phosphoproteome using an extended set of putative Gene Ontology (GO) annotations obtained from Ontology-based Pattern Identification (OPI) clustering [44]. GO terms enriched in the merozoite phosphoproteome (this study) were compared with enriched terms in the ensemble of schizont phosphoproteomes represented by 12,252 phosphorylation sites detected previously [18-22]. Statistical relevance in GO term enrichment between merozoites and schizonts was assessed by Fisher exact tests (Table S2). The GO terms more than two-fold enriched in the merozoite- relative to schizont-phosphoproteomes are shown in Figure 2. We note that the enriched GO terms ‘protein secretion’, ‘secretion’, and ‘secretion by cell’ were not found to be statistically relevant, and neither are GO terms represented by less than five proteins in the merozoite phosphoproteome (*e.g*. ‘ATPase

activity, coupled to transmembrane movement of ions' and 'rhoptry'), even though the differences appear striking.

In the category 'Molecular Function' (red columns, Figure 2 and see Table S3) we found differences between merozoites and schizonts for terms associated with phosphorylation such as 'lipid kinase activity' ($p < 0.05$) and 'calmodulin-dependent protein kinase activities' ($p < 0.1$), as well for 'protein degradation', 'threonine-type peptidase' and 'endopeptidase activities' ($p < 0.05$). GO terms in the category 'cellular components' (green columns) were enriched ($p < 0.1$) in invasion-related components such as 'apical part of cell' and 'apical complex' and significantly enriched ($p < 0.05$) for 'ubiquitin-mediated degradation' and 'proteasome core complex'. Finally, 16 biological process (blue columns) were identified as enhanced in the merozoite phosphoproteome including 11 with statistical relevance ($p < 0.05$) and 1 with $p<0.1$. These terms included 'cellular response to stress' and three terms related to 'movement and locomotion' that were most enriched ($p<0.05$) in the merozoite phosphoproteome.

A second functional enrichment analysis was carried out with manually curated pathways from the Metabolic Malaria Pathway database (MMPD) (http://priweb.cc.huji.ac.il/malaria/). Enrichment in the merozoite phosphoproteome was compared with enrichment in the ensemble of schizont phosphoproteomes (Figure 3; Table S3). More than two-fold difference in enrichment ($p < 0.05$) between merozoites and schizonts was observed for 'histone acetylation', and 'phosphoinositides and membrane traffic'. The first term suggests an epigenetic change in gene expression in merozoites. We previously highlighted extensive phosphatidyl inositol signalling in schizonts [18] and now with the identification of eleven phosphorylated proteins involved

396 in inositol phosphate metabolism the current analysis argues that phosphatidyl inositol
397 signalling is even more elevated in merozoites. This would likely strongly activate
398 phosphatidyl inositol 3-phosphate kinase (PI3K)/Vps34 [45]. Importantly, two terms
399 'Genes coding for components of the proteasome degradation machinery' and
400 'proteasome-mediated proteolysis of ubiquitinated proteins' were also significantly
401 enriched ($p < 0.05$).
402
403 **3.3 Protein interaction network of the merozoite phosphoproteome**
404 We demonstrated previously that specific phosphorylated protein complexes in *P.*
405 *falciparum* schizonts have the potential to regulate most of the biological activities at this
406 stage [18]. Therefore, the merozoite phosphoproteome was mapped onto predicted
407 protein-protein interactions from the STRING database [38] to construct a scale-free
408 protein-interaction network of phosphorylated merozoite proteins. STRING is a protein-
409 protein interaction database of known interactions (from high throughput experiments
410 and literature mining) and predicted interactions (from genomic context and co-
411 expression) currently covering approximately 1100 species including *P. falciparum*. The
412 constructed merozoite interactome is composed of 682 nodes/proteins covering 92% of
413 the phosphoproteome and 19,584 edges corresponding to protein-protein interactions.
414 The global interaction network was analysed for the presence of densely connected
415 sub-networks using the molecular complex detection (MCODE) clustering algorithm
416 [40]. This allowed the identification of 20 sub-networks (Table S4), with the majority
417 interconnected via the hub of 4 proteins present in MCODE 13 (Figure 4A). Putative
418 biological functions of the different MCODE clusters were assigned by MMPD

enrichment analyses, as described above. This resulted in potential functional annotations for 12 MCODE clusters representing 50% (369 proteins) of the merozoite phosphoproteome (Figure 4B). Their assignments are in good agreement with the MMPD enrichment analysis (Figure S1), and in some cases reinforced the proposed biological functions. For example, MCODE cluster 16 comprised of 4 phosphorylated proteins involved in inositol phosphate metabolism is 34-fold more enriched in the cluster than in the full merozoite phosphoproteome (Figure 4B). Similarly, the hub cluster MCODE 13 is 30-fold more enriched and is composed of three kinases (PF3D7_1428500, a putative GCN2; PF3D7_0515300 [PI3K]; and PF3D7_0610600, calcium dependent protein kinase 2 [CDPK2]), and the regulatory subunit (PF3D7_1223100) of cAMP-dependent protein kinase [PKA]).

MCODE cluster 1 was identified as the largest sub-network composed of 119 phospho-proteins with potentially 5739 protein-protein interactions (Figure 4A). It is under-represented in schizont phosphorylation sites ($p < 0.05$) (Table S4), indicating an enhanced role for this cluster in merozoite-related processes. Consistently, 23 proteins had MMPD terms such as ‘components of the linear motor responsible for merozoite motility in invasion’, ‘domains of merozoite surface proteins’, ‘functional annotation of merozoite invasion-related proteins’, ‘subcellular localization of proteins involved in invasion’ and ‘genes coding for GPI-anchored membrane proteins’. Interestingly, four proteins were associated with the ATG autophagic pathway (Figure 4B). Involvement of proteins in the MCODE 1 cluster with cell invasion was further supported by enrichment in GO annotations for 'locomotion and movement' (9.2-fold) covering 49 proteins of

442 which 13 were annotated to 'the apical complex' (12.0-fold), pointing again to a role in
443 invasion (Table S5). The functional significance for 'locomotion and movement' of this
444 sub-network was further supported by large differences in fold enrichment between
445 MCODE cluster 1 (9.2-fold) and the merozoite phosphoproteome (2.0-fold) showing that
446 these putative functions are concentrated in the sub-network. The detection of highly
447 enriched protein kinase activities for PKA (11.9-fold) and CDPK (9.3-fold) suggests a
448 regulatory role for these kinases in controlling MCODE cluster 1 activity. MCODE1
449 activities are likely co-regulated (depicted with yellow circles) by MCODE13 with for
450 example, PKAr of MCODE13 regulating PKAc catalytic activity in MCODE1 (see Fig.
451 S1). Similarly, the autophagy pathway may be co-regulated by MCODE 13 via direct
452 interaction of CDPK5 and PKAr with ATG8.
453 The presence in MCODE1 of PKG (PF3D7_1436600), GC$\alpha$ (PF3D7_1138400) and
454 PKAc (PF3D7_0934800), together with CDPK1 (PF3D7_0217500) and CDPK5
455 (PF3D7_1337800) indicates that in merozoites there is significant crosstalk between the
456 secondary messenger cyclic nucleotides and calcium [7, 8]. We have noted previously
457 that in schizonts both CDPK1 and GAP45 (PF3D7_1222700) could be phosphorylated
458 *in vitro* by PKA [18]. The presence of the putative zinc finger transcription factor KROX1
459 (PF3D7_1209300) in MCODE1 now suggests that this crosstalk could have a
460 transcriptional outcome, as cAMP and $Ca^{2+}$ surges do on activating the transcription
461 factor Creb in mammalian cells [46, 47].
462
463

### 3.4 Phosphorylation motif analysis.

The merozoite phosphoproteome data set described here together with an ensemble of the reported phosphoproteomes of schizonts [18-22] enabled us to compare schizont to merozoite phosphorylation motifs. Firstly, we compared phosphorylation motif classes based on their chemical properties using a decision tree previously applied to our schizont phosphoproteome [18] (Figure 5). The motif classes ‘basic-directed’ and ‘other’ are overrepresented in merozoites (fold-changes: 2.0 and 1.3, respectively) compared to schizonts, while acidic-, proline- and tyrosine–directed classes are underrepresented (fold-changes: -2.0, -1.5 and -7.3, respectively). Tyrosine phosphorylation is almost absent in merozoites with only 9 sites found, suggesting that tyrosine kinase activity may modify parasite proteins in schizonts, but not merozoites (see also Figure 6).

Secondly, phosphorylation sites identified in merozoites were classified using the phosphorylation motif finding algorithm MotifX [36]. We identified 33 phosphorylation motifs (Table S6) of which only five were reported in schizonts [18] [19, 21]. Within the top 10 most abundant motifs we find 5 variants of the core motif [K/R]xx[S/T] covering 32.4 % of all phosphopeptides detected in merozoites. The 33 motifs contain no acidic residues (Asp and Glu), in contrast to schizonts, where 14 motifs were rich in these residues [18]. When the 33 motifs were mapped to known kinase target sites using CompariMotif [37], several ambiguous matches were observed (Table S7). However, the core motif ([K/R]xx[S/T]) exactly matched to known calcium/calmodulin-dependent protein kinase II and PKA substrates, while imperfect matches were observed to other AGC kinases such as PKC, PKD, PKG and Akt/PKB.

A clear trend emerged among the top 8 most enriched phosphorylation sites implicating upregulated calcium/calmodulin-dependent protein kinase and PKA activities in merozoites compared to schizonts (Figure 5B). Furthermore, we found that MCODE cluster 1 was 1.4-fold ($p < 0.05$) enriched for sites with the [K/R]xx[S/T] core motif relative to the full merozoite phosphoproteome (Table S4). No other MCODE cluster was found to be statistically significantly enriched for either the core motif or merozoite specific sites (Table S4), strengthening the notion that cluster 1 is enriched for merozoite-specific functions.

### 3.5 Differential phosphorylation between schizonts and merozoites at the site-specific level.

The above global phospho-motif view of differential phosphorylation between schizonts and merozoites was confirmed at a specific phospho-site level by examining the phosphorylation status of Ser47 in MTIP (PF3D7_1246400), which is phosphorylated by CDPK1 [41]. Serine 47 (KPL*$S_{47}$) in MTIP occurs within the core motif ([K]/R]xx[*S]/T]) that we have shown above is enriched in merozoites. The specific anti-phospho-S47 antibody recognised MTIP in merozoites, but not in schizonts and this recognition was phosphatase sensitive, clearly identifying S47 of MTIP as being specifically phosphorylated only in merozoites (Figure 6A).

### 3.6 Experimental testing of phospho-motif enrichment analysis confirms differential phosphorylation between schizonts and merozoites *in vivo*

The differential distribution of specific phosphorylation motifs between schizont (S) and merozoite (M) proteins was also confirmed using a panel of commercial phospho-motif specific antibodies (Figure 6B). Remarkable differences in phosphorylation patterns between schizonts and merozoites were observed with antibodies specific for a typical PKA substrate (motif 3: RRx[pS/pT]), a typical PKB/Akt substrate (motif 4: Rxx[pS/pT]) and a typical PKD substrate (motif 11: LxRxx[pS/pT]). Notably, the abundant core motif [K/R]xx[pS/pT] identified by MotifX analysis (section 3.4) would be recognised by antibodies to phospho-motifs 3, 4 and 11 (Figure 6B). So, three independent phospho-motif specific antibodies show that the core motif (K/R]xx[S/T]) is distributed differently between schizont and merozoites proteins *in vivo*. Proteins containing phospho-tyrosine

were difficult to detect using a specific anti-phosphotyrosine antibody, consistent with detection of only 9 sites in the merozoite phosphoproteome.

### 3.7 Experimental testing of GO and MMPD enrichment analyses shows that proteins are highly ubiquitinated in merozoites compared to schizonts

Our various comparative bioinformatics analyses indicated that merozoites are enriched in phosphoproteins involved in 'cellular response to stress', 'proteasome core complex', 'proteasome-mediated proteolysis' (Figure 2), and the 'autophagic pathway' (Figure 4B); a collection of terms that suggested heightened ubiquitin-mediated protein degradation might be taking place in merozoites. To test this prediction we probed protein extracts prepared from schizonts (42- and 45-hours post-invasion) and free merozoites with an antibody reactive with both mono- and poly-ubiquitinated proteins (Figure 6C). In merozoites there was a very marked increase in the level of ubiquitination compared to schizonts.

## 4. Discussion

The *P. falciparum* life cycle is complex with dynamic protein phosphorylation at different stages. Following erythrocyte invasion the intracellular parasite develops through ring, trophozoite and schizont stages prior to the release of extracelluar merozoites that invade new erythrocytes. Signal transduction pathways regulating development of the intraerythrocytic parasite have been identified by large scale phosphorylation screens of particular stages with a focus on schizonts [18-22]. In this study we have generated a phosphoproteome of extracellular merozoites, and compared it with an ensemble of schizont phosphoproteomes [18-22]. We used a subtractive approach to identify differential protein phosphorylation in merozoites, and identified 785 sites phosphorylated in merozoites and 980 phosphorylation sites shared between merozoites and schizonts. The large number of phosphorylation sites detected in the ensemble of schizont phosphoproteomes (12,252) compared to the 1785 sites detected in merozoites indicates with a reasonable degree of certainty that the 785 sites described in this study are merozoite specific.

At the phosphopeptide level we observed large differences in the distribution of specific phosphorylation motifs, with 28 motifs not previously observed in schizonts. In addition, the core motif sequence [K/R]xx[pS/pT] was highly enriched in merozoites being contained in 35 % of the 28 phospho-motifs; a significant enrichment that directly implicates upregulated calcium-dependent protein kinase and cAMP-dependent PKA activities in the biology of merozoites. The overall differential distribution of phosphorylated motifs was confirmed *in vivo* using commercial specific phospho-motif

antibodies to probe schizont and merozoite protein extracts. Three independent anti-phospho-motif antibodies confirmed that schizonts and merozoites are differentially phosphorylated. Consistently, the core motif [K/R]xx[pS/pT] that's enriched in merozoites is common to all 3 phospho-motifs likely explaining some of the common phospho-bands identified by western blot. This global view of differential phosphorylation does not identify given phosphoproteins, so we examined S47 in MTIP, as this residue occurs within the core motif imbedded in KPL*SIE. A specific phospho-S47 antibody demonstrated that S47 in MTIP is clearly differentially phosphorylated between schizonts (off) and merozoites (on). Thus, *in vivo* differential phosphorylation occurs between schizonts and merozoites both at the site-specific and global levels.

We argue that differential phosphorylation translates into functional differences in parasite biology that are highlighted by comparative gene ontology and pathway enrichment analyses. In both cases we observed an increase in terms involved in invasion biology (Figure 3, Table S2 and Table S3). This finding was corroborated by cluster analysis of the merozoite phosphoprotein interaction network, where the largest MCODE cluster (119 proteins) is also enriched for invasion biology. Besides invasion biology we find the ATG autophagy pathway also enriched in MCODE1, and together these observations lead us to propose that developing merozoites undergo starvation-induced translational arrest, since they no longer have access to amino acids derived from haemoglobin degradation. The marked increased in ubiquitination is consistent with autophagic digestion of organelles no longer required by merozoites to invade. Organelle and protein degradation would provide the necessary nutrient (lipid and

amino acids) for merozoites to survive the hostile extracellular environment, before they elaborate a new food vacuole to digest host cell proteins such as haemoglobin [12, 13]. This upregulation of ubiquitination in extracellular merozoites compared to schizonts has not been reported previously; in an earlier study ubiquitination was examined in intracellular ring, trophozoite and schizont stages but merozoites were not included in this analysis [48].

**Acknowledgements**

This work was supported by the FP7 projects MALSIG (HEALTH-F3-2009-223044 – MALSIG) for EL, GL and AH and Network of Excellence EviMalaR (Health-2009-2.3.2-1-242095) to EL and AH. The AH laboratory was supported by the MRC (File Reference U117532067). Infrastructural support to the GL laboratory was provided by INSERM and CNRS and GL also acknowledges support from the ParaFrap network of excellence (ANR-11-LABX-0024). We gratefully acknowledge Hagai Ginsburg for providing MMPD spreadsheets for pathway enrichment analysis. The antibodies specific for phosphoSer47-MTIP were a kind gift from Dr Debbie Taylor. We thank the Nijmegen Proteomics Facility for usage of the LC-MS instrumentation to carry out this study.

## FIGURE LEGENDS

Figure 1: The merozoite phosphoproteome of *Plasmodium falciparum.*

A: Schematic overview of the phosphoproteome workflow. Steps in the workflow to identify phosphopeptides in protease digests derived from 2-3*$10^9$ purified *P. falciparum* merozoites. After lysis proteins were digested in solution with lysC and trypsin and partially purified using FASP. Peptides were fractionated by strong anion exchange (SAX) disks, enriched for phosphopeptides by $TiO_2$ and measured by liquid chromatography tandem mass spectrometry. Phosphopeptides were identified by Mascot database searches and validated by MaxQuant at 1 % FDR. A detailed description of the procedure is provided in Experimental Procedures.

B: Venn diagram depicting overlap in protein phosphorylation sites between merozoite and schizonts ensemble from previous studies [18-22].

Figure 2. GO annotation of the phosphoproteomes of asexual blood stages.

Comparative gene ontology enrichment analysis between the phosphoproteomes of merozoites and schizont stages. Enrichment is shown for OPI-GO terms relative to all 5500 *P. falciparum* proteins. Statistical significance was tested using a one–tailed Fisher exact test.

Figure 3. Pathway annotation of the phosphoproteomes of asexual blood stages.

Comparative pathway enrichment analysis between the phosphoproteomes of merozoites and schizont life cycle stages. Enrichment is shown for increased MMPD pathway terms relative to all 5500 *P. falciparum* proteins. Statistical significance was tested using a one–tailed Fisher exact test (FET). We accepted pathways with p (FET) < 0.005 in this figure. Pathways with lower significance (0.005 < p < 0.05) are provided in Table S3.

Figure 4. The protein interaction network of the merozoite phosphoproteome.

A: Sub-networks of the phosphoprotein interaction network in merozoites. Protein interaction data were downloaded from STRING and superimposed on the merozoite phosphoproteome. Twenty sub-networks were identified by the MCODE clustering algorithm. Here MCODE clusters are shown that interact with the central kinase cluster MCODE 13.

B: MMPD pathway annotation of all MCODE clusters. A pathway enrichment analysis was performed against the background of all 5500 proteins, and a clustering analysis was performed to display functional divergence between MCODE clusters. Enriched pathways in MCODE 1 are shown in yellow.

Figure 5: Protein phosphorylation motifs detected in merozoites.

A: Distribution of phosphorylation classes (acidic, basic, proline-directed, tyrosine and other) in blood stages with merozoites in blue bars and schizonts in red bars.

B: Core phosphorylation motifs from the top 10 most abundant motifs in merozoites represented by 13-mer sequence logos. Amino acids of the core motif sequence [K/R] x x [S/T] are highlighted by red boxes.

Figure 6. Differential phosphorylation and ubquitination of proteins in schizonts and merozoites.

A: Western blot of schizont (S) and merozoite (M) protein extracts probed with an antibody specific for phosphorylated Ser47 in MTIP. The antibody only reacted with MTIP in merozoite extracts despite the presence of the protein in both schizonts and merozoites. Treatment of the merozoite extract with phosphatase (+) abolished the antibody reactivity confirming that phosphorylation of Ser47 was essential for antibody recognition. The presence of MTIP in both schizont and merozoite extracts is displayed with an antibody raised to recombinant MTIP.

B: Western blot of schizont (S) and merozoite (M) protein extracts probed with phosphorylated phospho-motif-specific antibodies. The bands recognised by the antibodies specific to motifs 3, 4 and 11 showed a differential pattern between schizonts and merozoites, whereas the anti-phosphotyrosine antibody showed only weak reactivity with both schizont and merozoite extracts. Anti-CDPK1 antibodies were used as a loading control.

C: Western blot of schizont protein extracts made 42 and 45 h post-invasion together with protein extracts made from free merozoites (M), probed with an antibody to mono- and poly-ubiquitinated proteins. The strong reactivity with merozoite proteins indicates an increased level of ubiquitination in merozoites compared to schizonts. Anti-CDPK1 antibodies were used as a loading control in the bottom panel.

The mobility of molecular mass markers (in kDa) is indicated on the left side of the panels.

**Supplementary data**

**Table S1**: Phosphopeptide identification in the merozoite phosphoproteome.

**Table S2**: Gene Ontology enrichment results comparing the merozoite phosphoproteome with the schizont phosphoproteome ensemble.

**Table S3**: MMPD pathway enrichment comparing the merozoite phosphoproteome with the schizont phosphoproteome ensemble.

**Table S4**: List of MCODE proteins.

**Table S5**: GO enrichment results for MCODE cluster 1.

**Table S6**: Phosphorylation motifs detected in merozoites.

**Table S7**: Kinase substrates predicted by CompariMotif.

**Figure S1**. Protein- Protein Interactions between MCODE 1 and MCODE 13

## References


[1] Sturm, A., Amino, R., van de Sand, C., Regen, T., *et al.*, Manipulation of host hepatocytes by the malaria parasite for delivery into liver sinusoids. *Science* 2006, *313*, 1287-1290.

[2] Miller, L. H., Ackerman, H. C., Su, X. Z., Wellems, T. E., Malaria biology and disease pathogenesis: insights for new treatments. *Nature medicine* 2013, *19*, 156-167.

[3] Bannister, L. H., Mitchell, G. H., Butcher, G. A., Dennis, E. D., Cohen, S., Structure and development of the surface coat of erythrocytic merozoites of Plasmodium knowlesi. *Cell and tissue research* 1986, *245*, 281-290.

[4] Cowman, A. F., Berry, D., Baum, J., The cellular and molecular basis for malaria parasite invasion of the human red blood cell. *J Cell Biol* 2012, *198*, 961-971.

[5] Baum, J., Richard, D., Healer, J., Rug, M., *et al.*, A conserved molecular motor drives cell invasion and gliding motility across malaria life cycle stages and other apicomplexan parasites. *J Biol Chem* 2006, *281*, 5197-5208.

[6] Farrow, R. E., Green, J., Katsimitsoulia, Z., Taylor, W. R., *et al.*, The mechanism of erythrocyte invasion by the malarial parasite, Plasmodium falciparum. *Seminars in cell & developmental biology* 2011, *22*, 953-960.

[7] Dawn, A. S., S.; More, K.R.; Siddiqui, F.A.; Pachikara, N.; Ramdani, G.; Langsley, G.; Chitnis, C.E., The Central Role of cAMP in Regulating Plasmodium falciparum Merozoite Invasion of Human Erythrocytes. *PLoS Pathog* 2014, *10*, e1004520.

[8] Gao, X., Gunalan, K., Yap, S. S., Preiser, P. R., Triggers of key calcium signals during erythrocyte invasion by Plasmodium falciparum. *Nat Commun* 2013, *4*, 2862.

[9] Billker, O., Lourido, S., Sibley, L. D., Calcium-dependent signaling and kinases in apicomplexan parasites. *Cell Host Microbe* 2009, *5*, 612-622.

[10] Holder, A. A., Mohd Ridzuan, M. A., Green, J. L., Calcium dependent protein kinase 1 and calcium fluxes in the malaria parasite. *Microbes and infection / Institut Pasteur* 2012, *14*, 825-830.

[11] Gerald, N., Mahajan, B., Kumar, S., Mitosis in the human malaria parasite Plasmodium falciparum. *Eukaryot Cell* 2011, *10*, 474-482.

[12] Dluzewski, A. R., Ling, I. T., Hopkins, J. M., Grainger, M., *et al.*, Formation of the food vacuole in *Plasmodium falciparum*: a potential role for the 19 kDa fragment of merozoite surface protein 1 ($MSP1_{19}$). *PLoS One* 2008, *3*, e3085.

[13] Abu Bakar, N., Klonis, N., Hanssen, E., Chan, C., Tilley, L., Digestive-vacuole genesis and endocytic processes in the early intraerythrocytic stages of Plasmodium falciparum. *J Cell Sci* 2010, *123*, 441-450.

[14] Tomlins, A. M., Ben-Rached, F., Williams, R. A., Proto, W. R., *et al.*, Plasmodium falciparum ATG8 implicated in both autophagy and apicoplast formation. *Autophagy* 2013, *9*, 1540-1552.

[15] Gaur, D., Chitnis, C. E., Molecular interactions and signaling mechanisms during erythrocyte invasion by malaria parasites. *Current opinion in microbiology* 2011, *14*, 422-428.

[16] Jacot, D., Soldati-Favre, D., Does protein phosphorylation govern host cell entry and egress by the Apicomplexa? *International journal of medical microbiology : IJMM* 2012, *302*, 195-202.

[17] Lasonder, E., Treeck, M., Alam, M., Tobin, A. B., Insights into the Plasmodium falciparum schizont phospho-proteome. *Microbes and infection / Institut Pasteur* 2012, *14*, 811-819.

[18] Lasonder, E., Green, J. L., Camarda, G., Talabani, H., *et al.*, The Plasmodium falciparum schizont phosphoproteome reveals extensive phosphatidylinositol and cAMP-protein kinase A signaling. *J Proteome Res* 2012, *11*, 5323-5337.
[19] Pease, B. N., Huttlin, E. L., Jedrychowski, M. P., Talevich, E., *et al.*, Global analysis of protein expression and phosphorylation of three stages of Plasmodium falciparum intraerythrocytic development. *J Proteome Res* 2013, *12*, 4028-4045.
[20] Solyakov, L., Halbert, J., Alam, M. M., Semblat, J. P., *et al.*, Global kinomic and phospho-proteomic analyses of the human malaria parasite Plasmodium falciparum. *Nat Commun* 2011, *2*, 565.
[21] Treeck, M., Sanders, J. L., Elias, J. E., Boothroyd, J. C., The phosphoproteomes of Plasmodium falciparum and Toxoplasma gondii reveal unusual adaptations within and beyond the parasites' boundaries. *Cell Host Microbe* 2011, *10*, 410-419.
[22] Collins, M. O., Wright, J. C., Jones, M., Rayner, J. C., Choudhary, J. S., Confident and sensitive phosphoproteomics using combinations of collision induced dissociation and electron transfer dissociation. *Journal of proteomics* 2014, *103*, 1-14.
[23] Wek, R. C., Jiang, H. Y., Anthony, T. G., Coping with stress: eIF2 kinases and translational control. *Biochemical Society transactions* 2006, *34*, 7-11.
[24] Funderburk, S. F., Wang, Q. J., Yue, Z., The Beclin 1-VPS34 complex--at the crossroads of autophagy and beyond. *Trends in cell biology* 2010, *20*, 355-362.
[25] Harr, M. W., Distelhorst, C. W., Apoptosis and autophagy: decoding calcium signals that mediate life or death. *Cold Spring Harb Perspect Biol* 2010, *2*, a005579.
[26] Tudisca, V., Simpson, C., Castelli, L., Lui, J., *et al.*, PKA isoforms coordinate mRNA fate during nutrient starvation. *J Cell Sci* 2012, *125*, 5221-5232.
[27] Taylor, H. M., Grainger, M., Holder, A. A., Variation in the expression of a Plasmodium falciparum protein family implicated in erythrocyte invasion. *Infection and immunity* 2002, *70*, 5779-5789.
[28] Blackman, M. J., Purification of Plasmodium falciparum merozoites for analysis of the processing of merozoite surface protein-1. *Methods in cell biology* 1994, *45*, 213-220.
[29] Wisniewski, J. R., Zougman, A., Nagaraj, N., Mann, M., Universal sample preparation method for proteome analysis. *Nat Methods* 2009, *6*, 359-362.
[30] Kyono, Y., Sugiyama, N., Imami, K., Tomita, M., Ishihama, Y., Successive and selective release of phosphorylated peptides captured by hydroxy acid-modified metal oxide chromatography. *J Proteome Res* 2008, *7*, 4585-4593.
[31] Rappsilber, J., Ishihama, Y., Mann, M., Stop and go extraction tips for matrix-assisted laser desorption/ionization, nanoelectrospray, and LC/MS sample pretreatment in proteomics. *Anal Chem* 2003, *75*, 663-670.
[32] Cox, J., Mann, M., MaxQuant enables high peptide identification rates, individualized p.p.b.-range mass accuracies and proteome-wide protein quantification. *Nat Biotechnol* 2008, *26*, 1367-1372.
[33] Olsen, J. V., Mann, M., Improved peptide identification in proteomics by two consecutive stages of mass spectrometric fragmentation. *Proc Natl Acad Sci U S A* 2004, *101*, 13417-13422.
[34] Bauer, S., Grossmann, S., Vingron, M., Robinson, P. N., Ontologizer 2.0--a multifunctional tool for GO term enrichment analysis and data exploration. *Bioinformatics* 2008, *24*, 1650-1651.
[35] Huttlin, E. L., Jedrychowski, M. P., Elias, J. E., Goswami, T., *et al.*, A tissue-specific atlas of mouse protein phosphorylation and expression. *Cell* 2010, *143*, 1174-1189.

[36] Schwartz, D., Gygi, S. P., An iterative statistical approach to the identification of protein phosphorylation motifs from large-scale data sets. *Nat Biotechnol* 2005, *23*, 1391-1398.
[37] Edwards, R. J., Davey, N. E., Shields, D. C., CompariMotif: quick and easy comparisons of sequence motifs. *Bioinformatics* 2008, *24*, 1307-1309.
[38] Szklarczyk, D., Franceschini, A., Kuhn, M., Simonovic, M., *et al.*, The STRING database in 2011: functional interaction networks of proteins, globally integrated and scored. *Nucleic Acids Res* 2011, *39*, D561-568.
[39] Shannon, P., Markiel, A., Ozier, O., Baliga, N. S., *et al.*, Cytoscape: a software environment for integrated models of biomolecular interaction networks. *Genome Res* 2003, *13*, 2498-2504.
[40] Bader, G. D., Betel, D., Hogue, C. W., BIND: the Biomolecular Interaction Network Database. *Nucleic Acids Res* 2003, *31*, 248-250.
[41] Green, J. L., Rees-Channer, R. R., Howell, S. A., Martin, S. R., *et al.*, The motor complex of Plasmodium falciparum: phosphorylation by a calcium-dependent protein kinase. *J Biol Chem* 2008, *283*, 30980-30989.
[42] Perkins, D. N., Pappin, D. J., Creasy, D. M., Cottrell, J. S., Probability-based protein identification by searching sequence databases using mass spectrometry data. *Electrophoresis* 1999, *20*, 3551-3567.
[43] Thingholm, T. E., Jensen, O. N., Larsen, M. R., Enrichment and separation of mono- and multiply phosphorylated peptides using sequential elution from IMAC prior to mass spectrometric analysis. *Methods Mol Biol* 2009, *527*, 67-78, xi.
[44] Zhou, Y., Ramachandran, V., Kumar, K. A., Westenberger, S., *et al.*, Evidence-based annotation of the malaria parasite's genome using comparative expression profiling. *PLoS One* 2008, *3*, e1570.
[45] Vaid, A., Ranjan, R., Smythe, W. A., Hoppe, H. C., Sharma, P., PfPI3K, a phosphatidylinositol-3 kinase from Plasmodium falciparum, is exported to the host erythrocyte and is involved in hemoglobin trafficking. *Blood* 2010, *115*, 2500-2507.
[46] Poser, S., Storm, D. R., Role of Ca2+-stimulated adenylyl cyclases in LTP and memory formation. *International journal of developmental neuroscience : the official journal of the International Society for Developmental Neuroscience* 2001, *19*, 387-394.
[47] Shaywitz, A. J., Greenberg, M. E., CREB: a stimulus-induced transcription factor activated by a diverse array of extracellular signals. *Annu Rev Biochem* 1999, *68*, 821-861.
[48] Ponts, N., Saraf, A., Chung, D. W., Harris, A., *et al.*, Unraveling the ubiquitome of the human malaria parasite. *J Biol Chem* 2011, *286*, 40320-40330.

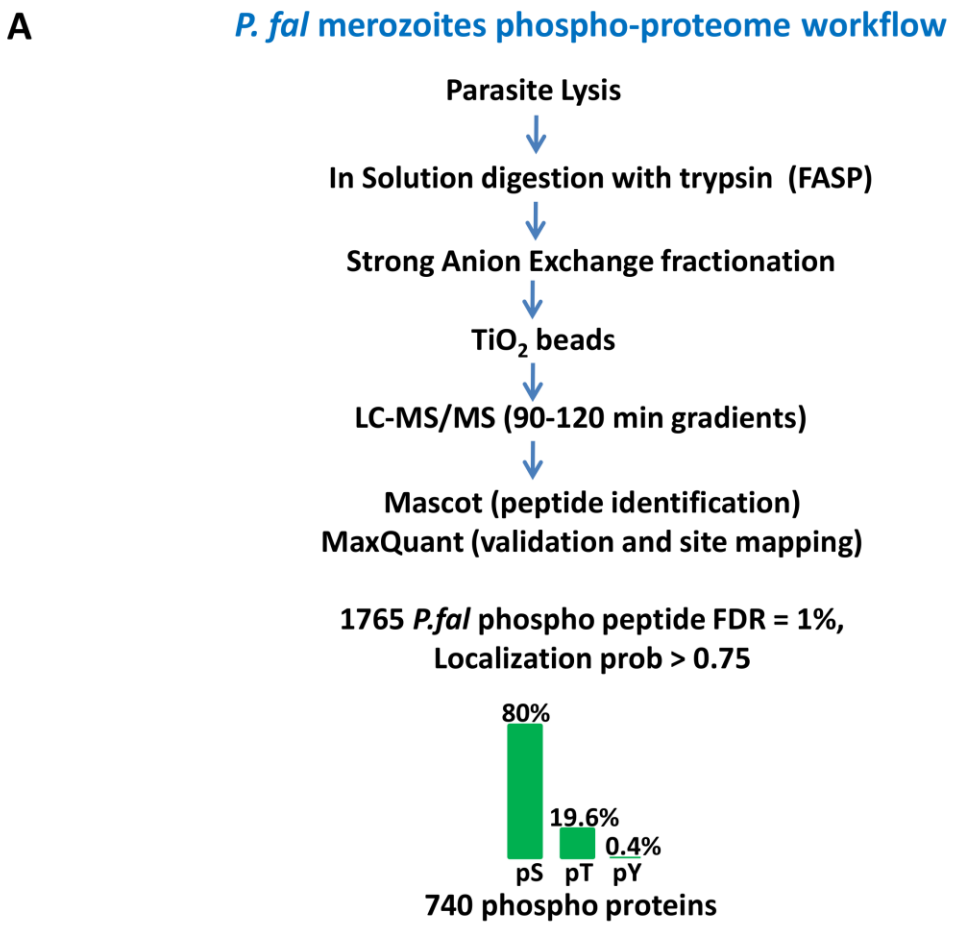


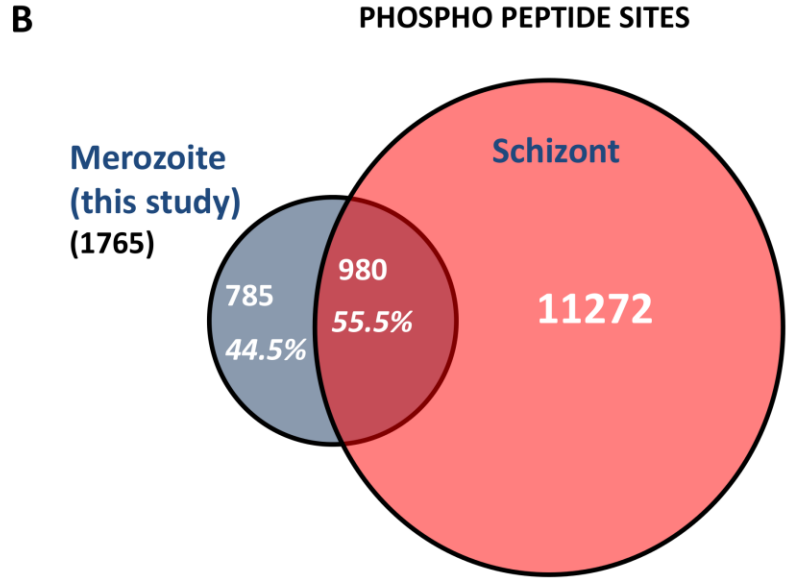


813
814 FIGURE 1

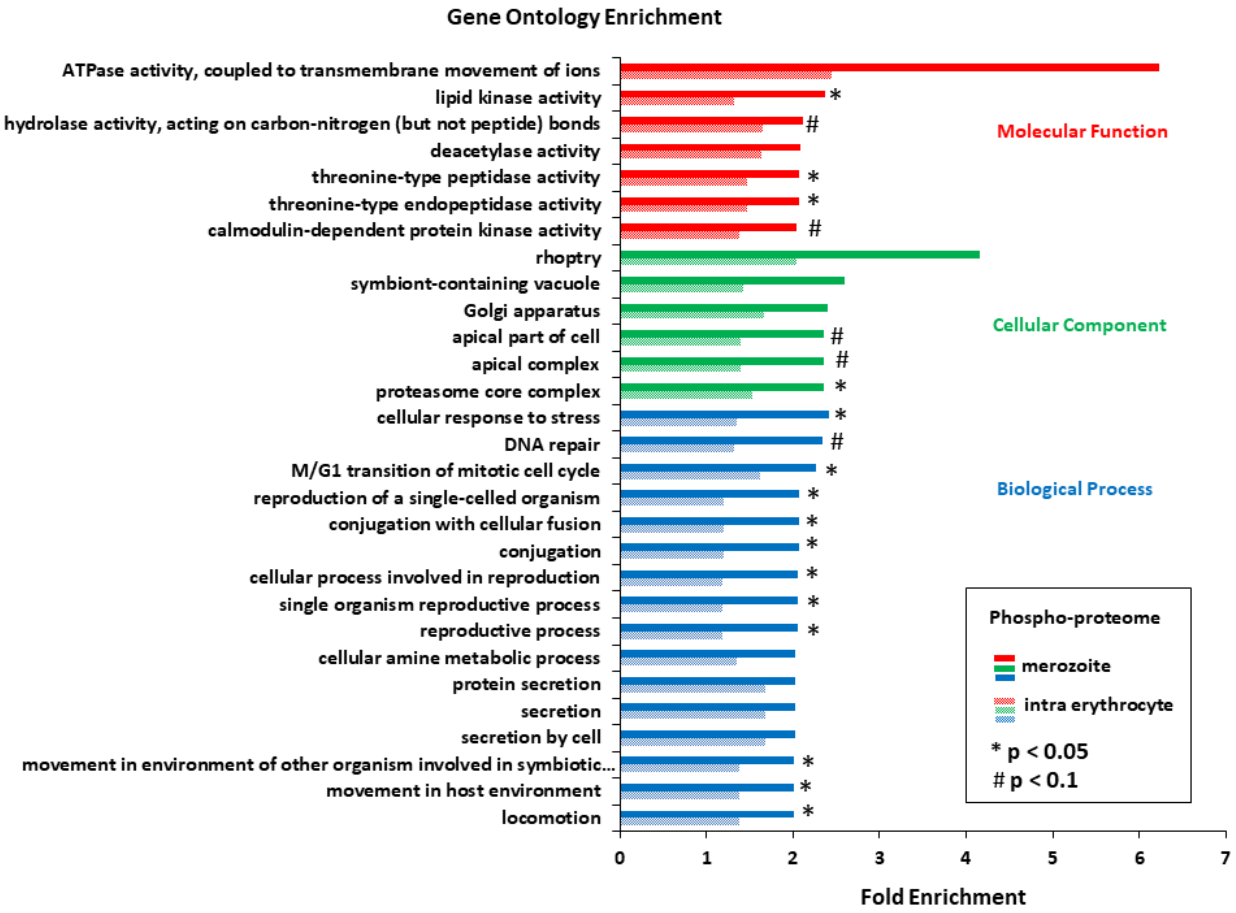
Gene Ontology Enrichment
ATPase activity, coupled to transmembrane movement of ions
lipid kinase activity
hydrolase activity, acting on carbon-nitrogen (but not peptide) bonds
deacetylase activity
threonine-type peptidase activity
threonine-type endopeptidase activity
calmodulin-dependent protein kinase activity
rhoptry
symbiont-containing vacuole
Golgi apparatus
apical part of cell
apical complex
proteasome core complex
cellular response to stress
DNA repair
M/G1 transition of mitotic cell cycle
reproduction of a single-celled organism
conjugation with cellular fusion
conjugation
cellular process involved in reproduction
single organism reproductive process
reproductive process
cellular amine metabolic process
protein secretion
secretion
secretion by cell
movement in environment of other organism involved in symbiotic...
movement in host environment
locomotion
Molecular Function
Cellular Component
Biological Process
Phospho-proteome
merozoite
intra erythrocyte
* p < 0.05
# p < 0.1
0
1
2
3
4
5
6
7
Fold Enrichment

FIGURE 2

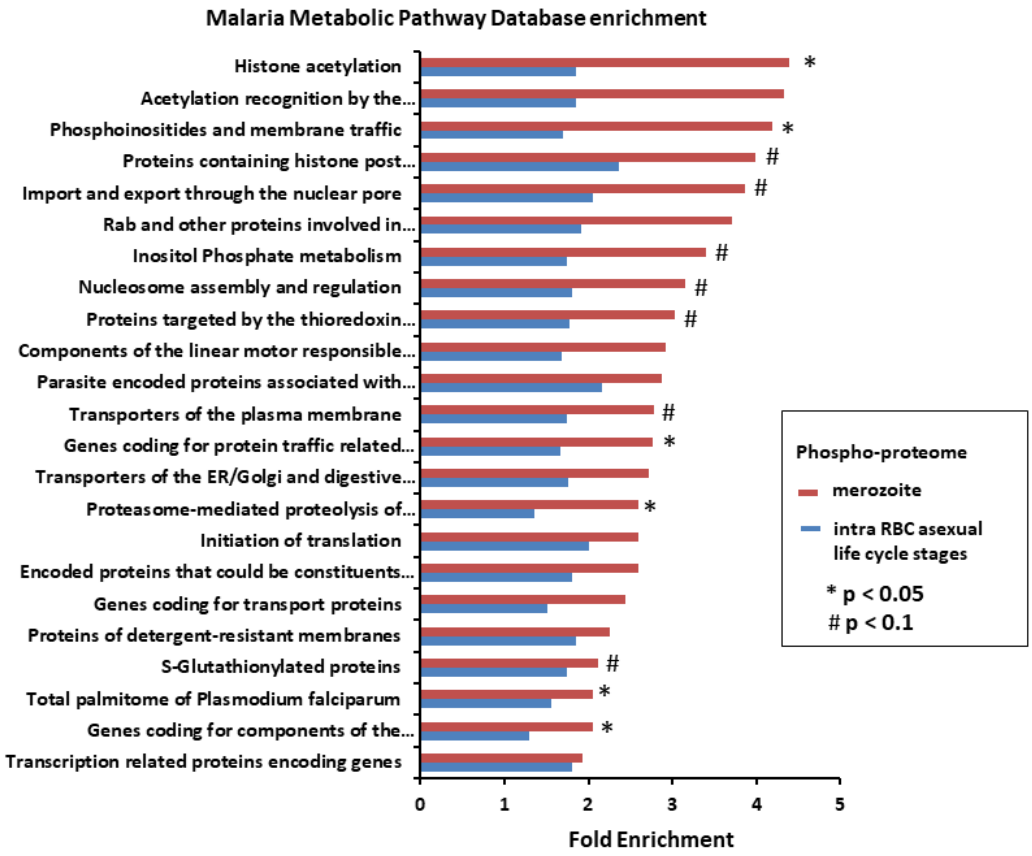


826

827 FIGURE 3

828

829

830

831

832

833

834

835

836

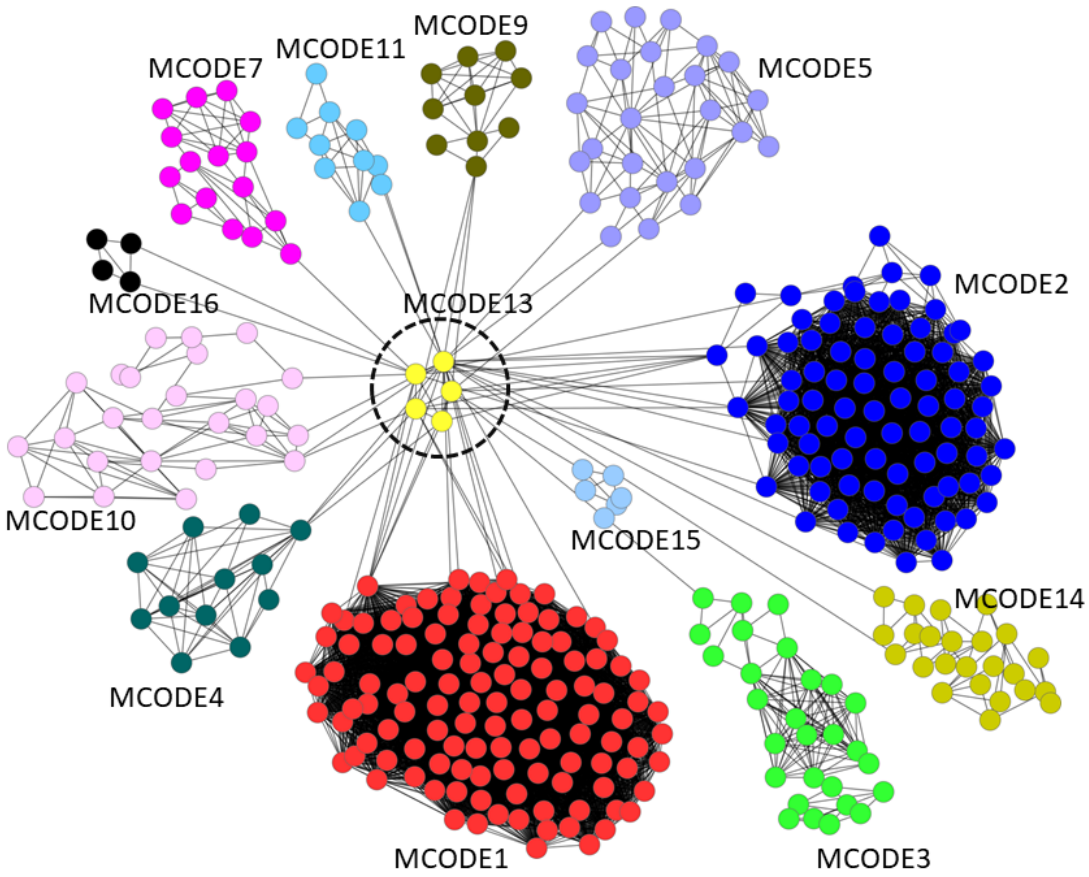
MCODE9
MCODE11
MCODE7
MCODE5
MCODE16
MCODE13
MCODE2
MCODE10
MCODE15
MCODE14
MCODE4
MCODE1
MCODE3

FIGURE 4A

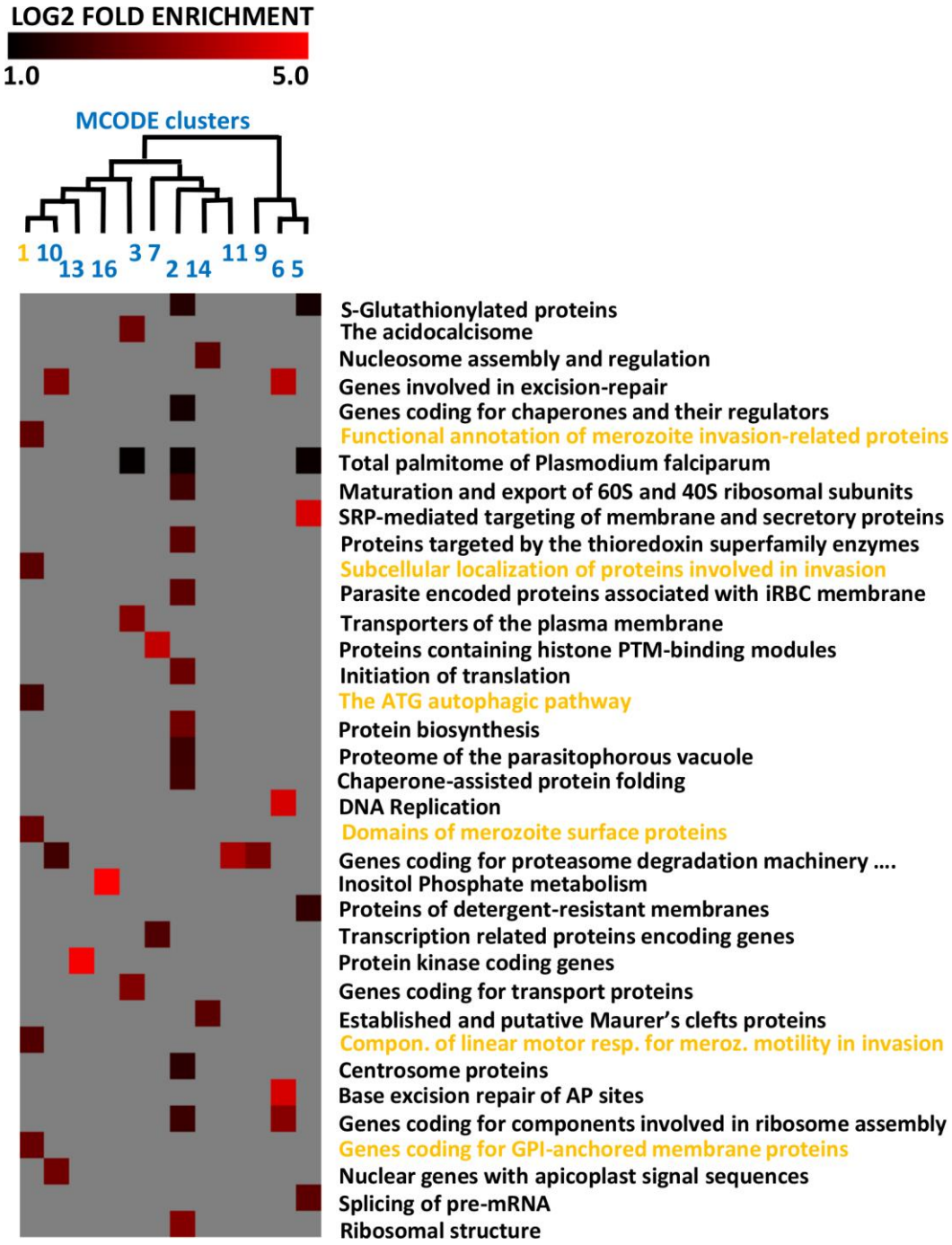
LOG2 FOLD ENRICHMENT
1.0
5.0
MCODE clusters
1 10 13 16 3 7 2 14 11 9 6 5
S-Glutathionylated proteins
The acidocalcisome
Nucleosome assembly and regulation
Genes involved in excision-repair
Genes coding for chaperones and their regulators
Functional annotation of merozoite invasion-related proteins
Total palmitome of Plasmodium falciparum
Maturation and export of 60S and 40S ribosomal subunits
SRP-mediated targeting of membrane and secretory proteins
Proteins targeted by the thioredoxin superfamily enzymes
Subcellular localization of proteins involved in invasion
Parasite encoded proteins associated with iRBC membrane
Transporters of the plasma membrane
Proteins containing histone PTM-binding modules
Initiation of translation
The ATG autophagic pathway
Protein biosynthesis
Proteome of the parasitophorous vacuole
Chaperone-assisted protein folding
DNA Replication
Domains of merozoite surface proteins
Genes coding for proteasome degradation machinery ....
Inositol Phosphate metabolism
Proteins of detergent-resistant membranes
Transcription related proteins encoding genes
Protein kinase coding genes
Genes coding for transport proteins
Established and putative Maurer's clefts proteins
Compon. of linear motor resp. for meroz. motility in invasion
Centrosome proteins
Base excision repair of AP sites
Genes coding for components involved in ribosome assembly
Genes coding for GPI-anchored membrane proteins
Nuclear genes with apicoplast signal sequences
Splicing of pre-mRNA
Ribosomal structure

FIGURE 4B

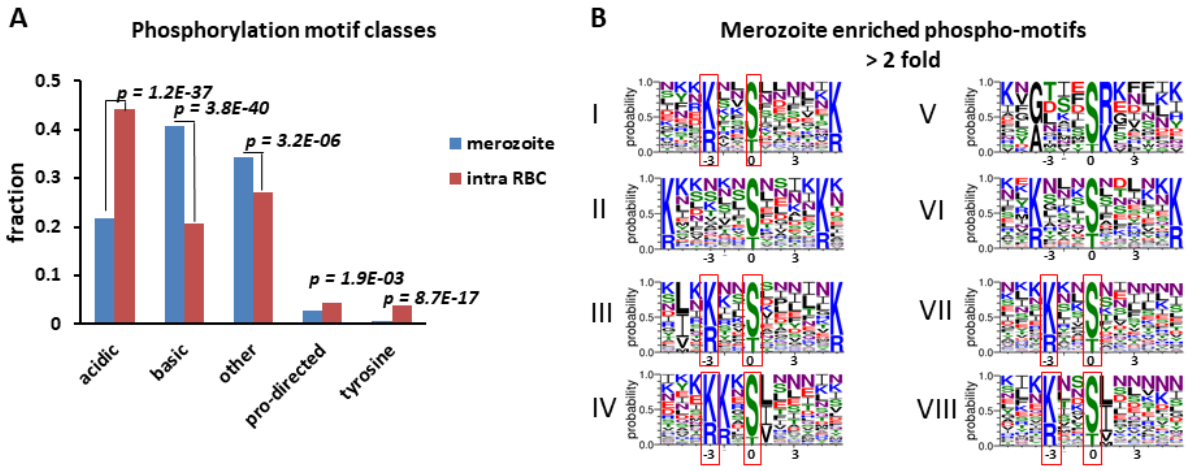


850

851 FIGURE 5

852

853

854

855

856

857

858

859

860

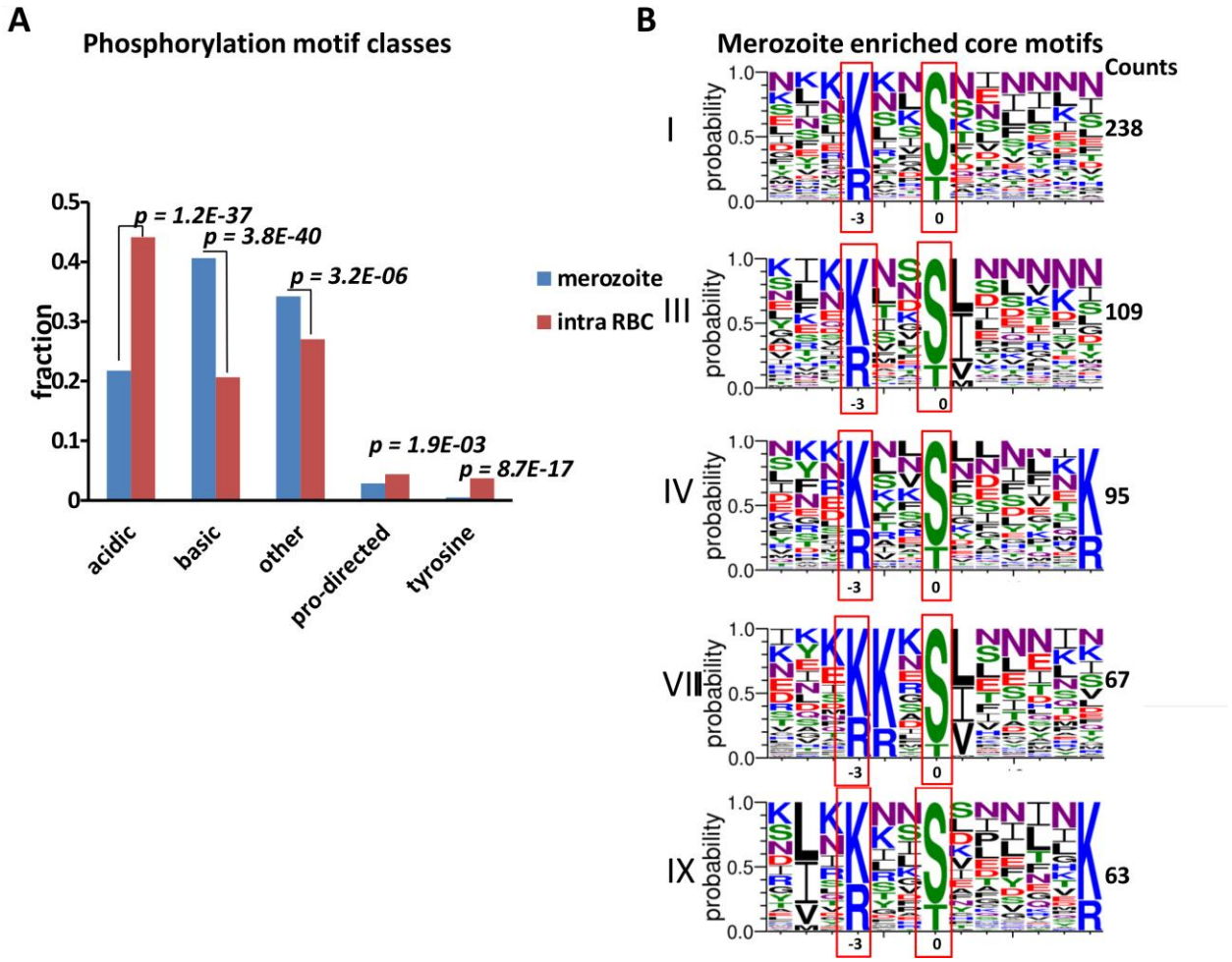
A
Phosphorylation motif classes
fraction
0.5
0.4
0.3
0.2
0.1
0
p = 1.2E-37
p = 3.8E-40
p = 3.2E-06
p = 1.9E-03
p = 8.7E-17
merozoite
intra RBC
acidic
basic
other
pro-directed
tyrosine
B
Merozoite enriched core motifs
Counts
I
238
III
109
IV
95
VII
67
IX
63
probability
1.0
0.5
0.0
-3
0

FIGURE 6A

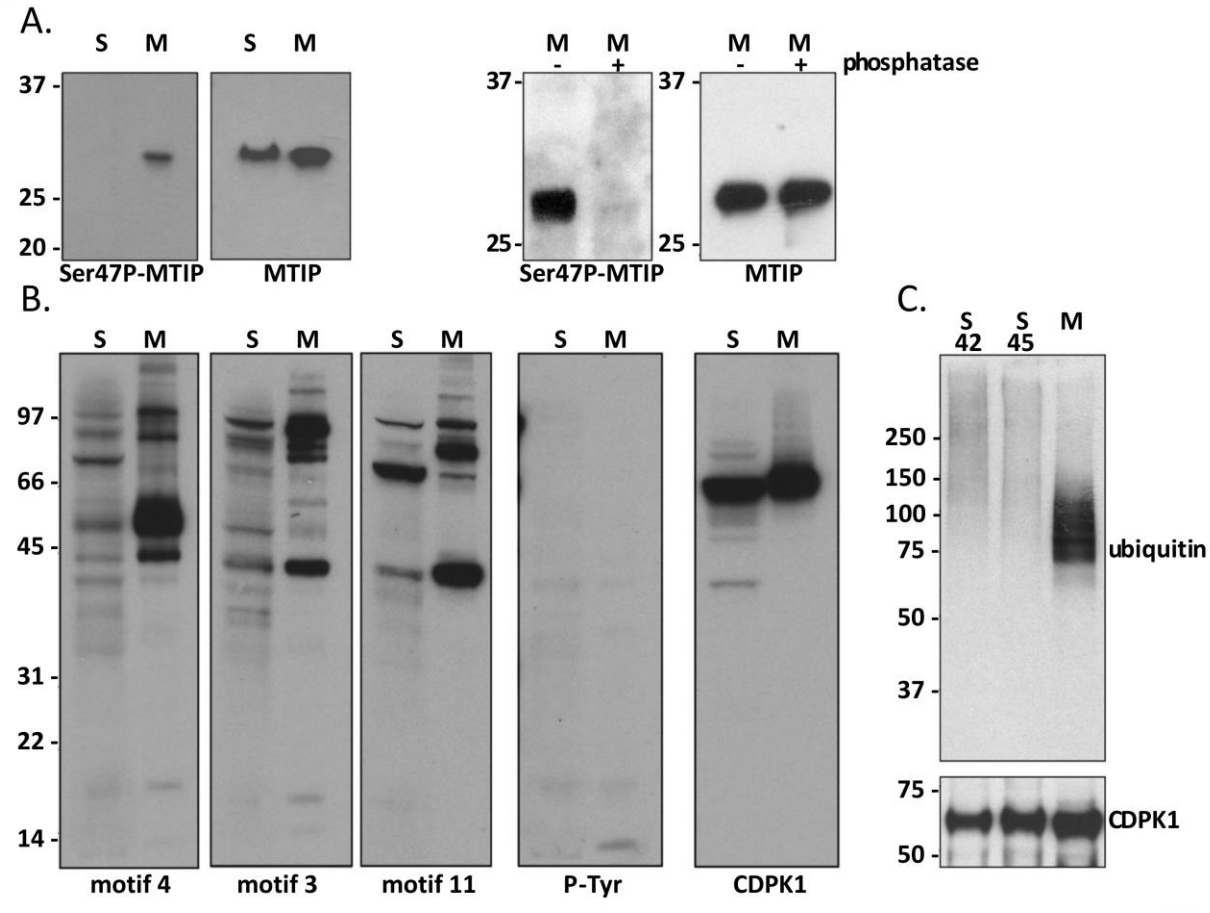
A.
S M S M
37
25
20
Ser47P-MTIP
MTIP
M M M M
- + - +
phosphatase
37
25
37
25
Ser47P-MTIP
MTIP
B.
S M S M S M S M S M
97
66
45
31
22
14
motif 4
motif 3
motif 11
P-Tyr
CDPK1
C.
S S M
42 45
250
150
100
75
50
37
ubiquitin
75
50
CDPK1

FIGURE 6B

FiGURE S1. Protein- Protein Interactions between MCODE 1 and MCODE 13

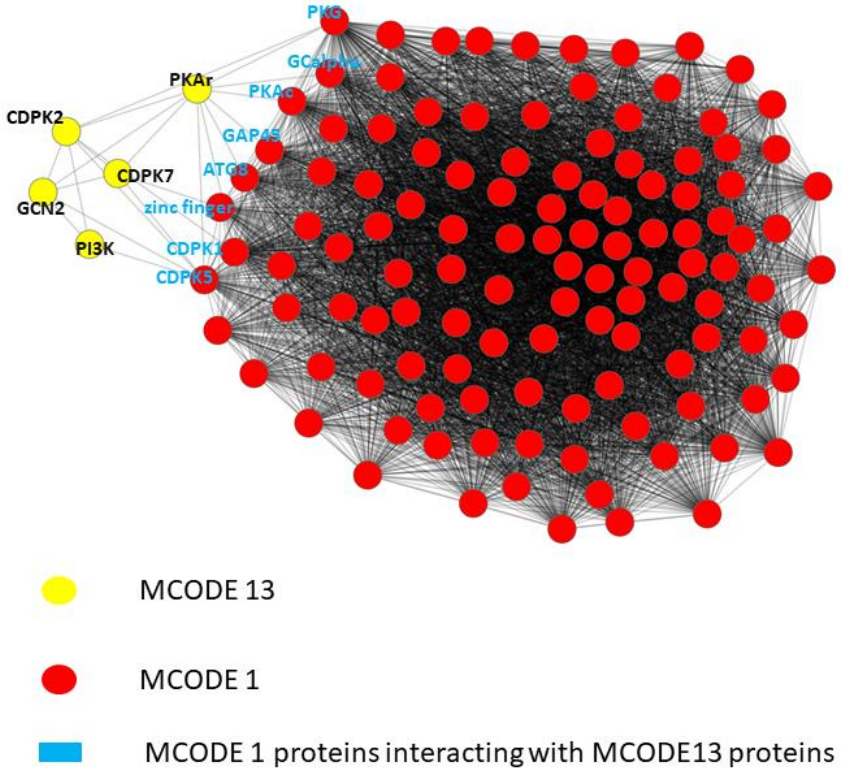


883